

Pinching of gel-filled honeycomb

Faezeh Shalchy*, Jenny Carlsson*, Vikram Deshpande*, Norman Fleck**

* Cambridge University Engineering Dept., Trumpington St., Cambridge, CB2 1PZ, UK

+ Corresponding author. Email: naf1@eng.cam.ac.uk FAX: +44 1223 332662

Abstract

The effect of gel-filling of a hexagonal honeycomb upon its transverse compressive response is investigated experimentally and numerically. The specimens comprise square tubes with sealed ends and are made from aluminium alloy honeycomb. The specimens are loaded transversely between frictionless flat platens at their mid-length. First, the measured pinch strength of the square tube made from empty honeycomb material is compared with the in-plane, uniaxial compressive response of the honeycomb. Finite element simulations confirm that the pinched honeycomb forms a series of crush bands at an approximately constant applied load. The elevation in compressive strength of the empty pinched tubes, compared to the uniaxial compressive strength of the honeycomb, is due to the development of membrane axial tension in the honeycomb external to the pinched zone. It is then shown experimentally and by finite element simulation that gel-filling of the hexagonal honeycomb in the closed-ended tubes changes the deformation mode in the pinched zone from that of the empty honeycomb. The pinch load increases with increasing displacement, with no evidence of crush band formation. The highly stable response is due to the presence of the incompressible gel-core, and due to the build-up of membrane tension, in the axial direction, within the walls of the honeycomb. As pinching proceeds, axial flow of the gel occurs from the shrinking, pinched zone to the outer, free-standing, dilating portions of the tube. The peak pinch force is limited in the experimental study by failure of the end-plugs of the tube and by necking of the cell walls of the honeycomb, particularly at the edge of the loading platen. Additional finite element simulations quantify the sensitivity of pinch strength to the inclination of the cell walls of the honeycomb, and to the presence of geometric imperfections within the honeycomb. Reference 2D calculations of the in-plane compression of the filled and empty honeycombs confirm that elimination of formation of the crush bands in the gel-filled honeycomb is due to the incompressibility of the core.

Keywords: pinching test, hexagonal honeycomb, lattice materials

1. Introduction

The hexagonal honeycomb is ubiquitous in both engineering applications and in the natural world. Examples in nature range from wood cells to the wax honeycomb of the honeybee, as first noted by Robert Hooke in 1665. Engineering examples range from the core of sandwich panels in aerospace to energy absorbing structures in crash mitigation. The underlying mechanics of the hexagonal honeycomb is contained within the seminal monograph by Gibson and Ashby (1997). They explain that the mechanical properties of the hexagonal honeycomb, such as Young's modulus and compressive strength, are highly anisotropic such that the axial properties scale with relative density whereas the transverse properties scale with relative density to a power of 2 for strength and 3 for modulus. The present study explores the elevation in transverse compressive strength of a hexagonal honeycomb upon filling of the cells of the honeycomb by an incompressible gel of negligible strength.

An extensive literature exists on the mechanics of *empty* honeycombs, see for example Gibson and Ashby (1997). Initial yield occurs by the formation of plastic hinges, and a softening response ensues due to geometric softening. Papka and Kyriakides (1994, 1998) showed that the compressive response involves the formation of a series of crush bands. Although the initiation of crushing is sensitive to specimen geometry and to the presence of geometric imperfections, the level of compressive stress that is required to broaden the crush bands, by the successive collapse of neighbouring layers of honeycomb, is almost insensitive to the presence of the imperfections and is adequately predicted by the so-called Maxwell stress for steady state propagation of an instability. This plateau stress for propagation of the instability can be determined by a straightforward energy argument, see Kyriakides (1993) or Papka and Kyriakides (1994) for details. As fully recognised by Kyriakides (1993), this approach has several caveats, for example it neglects the non-proportional strain path experienced by material elements as a crush band propagates, and it neglects the effect of strain rate and material inertia. Whilst Gibson and Ashby (1997) emphasised the significance of the yield strength of an elastic, ideally plastic honeycomb, and Papka and Kyriakides (1994) emphasised the subsequent formation of crush bands, an intermediate phenomenon also exists: plastic bifurcation of the honeycomb into periodic buckling modes. Triantafyllidis and Schraat (1998) explored this phenomenon by Bloch wave analysis, and generated failure surfaces on this basis.

Now consider a honeycomb filled with a second phase and ask whether the presence of the filled core has a major effect upon its in-plane compressive response. There is a limited literature on the mechanics of transverse crushing of a filled honeycomb. D'Mello and Waas (2013) explored

the in-plane compressive response of a circular cell, hexagonally packed, thin-wall polycarbonate (PC) honeycomb in two states: empty and filled with a PDMS elastomer. They found that the mode of crushing and the crush strength are sensitive to the presence of the PDMS core. In the unfilled state, the honeycomb undergoes progressive row-wise collapse at almost constant applied stress. In contrast, in the filled state, the response is stable with a monotonically increasing load versus displacement response and no evidence of localisation by crush band formation. Note that the compressive strength of the PDMS alone much exceeds that of the empty PC honeycomb, and so it is unclear whether the change in collapse mode upon filling of the honeycomb by a core material is due to the relative strength of the two materials or due to the incompressibility constraint imposed by the core.

Additional insight can be obtained from the study of Mozafari et al. (2015). They measured the in-plane compressive response of an aluminium hexagonal honeycomb, filled with a compressible polyurethane foam. Again, this core material has a larger compressive strength than that of the empty honeycomb, and the compressive strength of as-filled honeycomb much exceeds the rule-of-mixtures estimate. However, for this choice of material system, crush bands form in both the empty and polyurethane foam-filled hexagonal honeycomb, implying that there is no change in collapse mode due to the presence of the core. This suggests that the switch in collapse mode from crush band formation to a stable, uniform response in the D'Mello and Waas (2013) tests is due to the incompressible nature of the core. The purpose of the present study is to test this hypothesis by considering an incompressible core that is much weaker than the empty honeycomb.

The present study builds upon the recent analysis by Tankasala et al. (2021) of the small-strain, in-plane, elasto-plastic response of a hexagonal honeycomb using slender beam theory; incompressibility of the honeycomb was enforced by filling the core of the honeycomb with an incompressible and inviscid fluid. They assumed that the relative density of the honeycomb is sufficiently small for the struts to behave as Euler-Bernoulli slender beams. Exact solutions were obtained for the elastic moduli and for the macroscopic yield surface of the rigid, ideally plastic honeycomb under general in-plane loading: the solutions satisfy equilibrium, compatibility and the constitutive response of each elastic, ideally plastic beam. Macroscopic compressive straining of the incompressible honeycomb requires the stretching of the cell walls in addition to bending, and the modulus and compressive strength of the incompressible honeycomb are thereby elevated. Tankasala et al. (2021) obtained explicit analytical formulae for the macroscopic modulus and strength of the incompressible honeycomb. We emphasise that this analytical study, although exact, considers only the initial small strain response and assumes that the core neither cavitates nor separates from the cell walls of the honeycomb so that the macroscopic response is

incompressible. Both restrictions are relaxed in the present study; further, the present study is both experimental and numerical in nature.

A limited number of studies have considered the role of core filling upon the *out-of-plane* collapse response of a hexagonal honeycomb. Vaziri et al. (2006) performed a finite element analysis of a sandwich plate comprising a square or triangular honeycomb. They quantified the small enhancement in honeycomb performance under crushing and impulsive loads by the addition of a polymer foam to the honeycomb. They found that the foam-filled honeycomb gives negligible advantage over the unfilled honeycomb based on a fixed total weight of a sandwich plate with the honeycomb core.

The above considerations motivate the present study: does the filling of a hexagonal honeycomb by an incompressible core of vanishing shear strength have a significant influence upon the in-plane collapse response, and lead to a switch in collapse mechanism from crush band formation to a stable, homogeneous response?

Scope of Study

The present study explores the 3D structural response of a square tube made from an unfilled hexagonal honeycomb, and of a gel-filled hexagonal honeycomb (with suitable end sealing of the tube). The tube is pinched transversely over a finite portion at its mid-length, and the pinch force versus displacement response is both measured and predicted by finite element simulations. Detailed simulations are performed to determine whether the mode of deformation changes due to the presence of the gel core, and whether there is a consequent effect upon the pinch strength.

2. Materials and Methods

Specimens were made from commercially available Al 5052-H32 hexagonal honeycomb¹ of thickness $t = 35 \mu\text{m}$, supplied in the following as-manufactured manner. Epoxy stripes were printed on the Al 5052-H32 foils; the foils were then stacked and hot pressed to allow the adhesive to cure and bond the sheets together to form a block honeycomb. Expansion of this block generated the open honeycomb structure. The perfect honeycomb structure is sketched in Fig. 1b with the hexagonal cell structure lying in the $y - z$ plane while the axial direction of the hexagonal tubes is along the x -direction, see Fig. 1a. The perfect honeycomb has cell walls of thickness $2t$ and

¹ Corex honeycomb, 5 Stukeley Business Centre, Blackstone Road, Huntingdon, Cambridgeshire, PE29 6EF, UK

length h along the y – direction and walls of thickness t and length ℓ inclined at an angle ω with respect to the z – direction (Fig. 1b). However, imperfections introduced during manufacture implied that the microstructure of the as-received honeycombs is irregular. We conducted image analysis of 300 cells of the as-received honeycomb samples which revealed that the microstructure is characterised by average values of cell wall dimension $\bar{\ell} = 2.1$ mm and $\bar{h} = 1.7$ mm and cell wall inclination $\bar{\omega} = 35^\circ$. The relative density (density of smeared-out honeycomb to the density of the solid Al) of the honeycomb samples was measured to be $\bar{\rho} = 0.027$. Prismatic honeycomb specimens of cross-section 7×8 cells in the $y - z$ plane, and length $L = 200$ mm in the x – direction, were cut from the expanded honeycomb blocks. The microstructure implies that the tubes have an approximately square cross-section of side H with $H = 30$ mm. The honeycombs were tested in the as-received, empty state and in a gel-filled state, using a filling procedure as described in the following section.

2.1 *Manufacture of fluid-filled honeycomb specimens*

We manufactured tubular honeycomb specimens filled with an incompressible low viscosity gel. The gel was made by mixing 42g of a standard commercial gelatine powder with approximately 1 litre of water. The gel was inserted into the empty honeycomb as follows. One end of the tubular honeycomb specimen was plugged using Opti-tec 5001 optical epoxy adhesive². After the plug had cured, the specimen was made to stand vertically, with the open end at the top and the gel in the uncured state syringed into the individual tubes of the honeycomb. After the gel had set, the top of the specimen was also plugged via the Opti-tec 5001 epoxy adhesive to give the specimen sketched in Fig. 2.

2.2 *Test protocol*

Pinch tests were performed on both empty tubes (with free ends) and gel-filled tubes (with epoxy-sealed ends) as follows. Cuboidal steel indenters of dimension W in the x – direction and $2H = 60$ mm in the z – direction were used to centrally pinch the tubular specimens at a rate $\dot{u}/H = 6 \times 10^{-4} \text{ s}^{-1}$ in the y – direction, as shown in Fig. 1a. The contacting surfaces between the indenter and the honeycomb were sprayed with PTFE spray to reduce friction and loading was carried out in a screw-driven test machine. The relative displacement u between the two indenters was measured via a laser extensometer while the applied compressive load F was

² Intertronics, Station Field Industrial Estate, Oxford, OX5 1JD, UK.

measured using the load cell of the test machine. The indenter size was varied over the range $0.05 \leq W/L \leq 1$, for empty honeycombs. Here, $W/L = 1$ denotes uniaxial compression of the honeycomb in the y – direction (and for this choice $L = 30$ mm). Only pinching experiments with $W/L = 0.1$ and 0.25 were conducted on the filled specimens; the constraint imposed by the end plugs means that it was not possible to perform uniaxial compression tests on the filled specimens. Photographs of the specimens were taken throughout the tests to observe the deformed profiles of the specimens in the $x - y$ plane. At least 3 repeat tests were conducted in each case.

3. Experimental results

3.1 Response of the empty honeycomb

The measured pinching response of the honeycomb tubes is plotted in Fig. 3a in terms of the normalised load $F/(WH)$ versus normalised relative displacement u/H of the indenters for indenter sizes in the range $0.05 \leq W/L \leq 1$. Three independent measurements were conducted in each case, and we show one representative curve in Fig. 3a along with a shaded band showing the variability over the three tests.

First, consider the uniaxial compressive response ($W/L = 1$). Consistent with a large body of measurements (see for example Papka and Kyriakides (1994), as discussed in the Introduction), we observe an initial elastic part followed by a regime where the nominal stress given by $F/(WH)$ remains approximately constant. This constant, plateau stress, is associated with the formation and broadening of crush bands within the honeycomb.

Second, consider the pinching response for $0.05 \leq W/L \leq 0.25$. The response is qualitatively different from the uniaxial case with the normalised load versus displacement displaying hardening, in addition to oscillations in load associated with crush band formation between the indenters. The hardening rate increases with decreasing W/L such that the normalised load $F/(WH)$ increases with decreasing W/L for any given u/H . The source of the hardening can be understood from sketches of the observed longitudinal profiles of the $W/L = 0.25$ specimen included in Fig. 4: a photograph of the specimen in the experimental setup is included in Fig. 4a while in Fig. 4b we show outlines of the longitudinal profiles with increasing u/H . These outlines clearly show longitudinal stretching (along the $x -$ direction) of the honeycomb cell walls and we attribute the hardening to membrane action in the stiff longitudinal direction of the honeycomb; such membrane action is absent under uniaxial compression. The degree of stretching increases with decreasing W/L resulting in the observed increase in the associated hardening rate.

3.2 Response of the filled honeycomb

The measured $F/(WH)$ versus u/H response of the $W/L = 0.25$ filled specimen is included in Fig. 5a. Again, we conducted three independent measurements and we show in Fig. 5a a representative measurement along with a shaded band that indicates the variability over the three tests. The filled specimen has a nearly linear $F/(WH)$ versus u/H response over the range of displacements investigated here (leaking of the gel from the end plugs prevented investigation to larger deformations). A photograph of the specimen in the experimental setup is included in Fig. 6a while outline sketches of the longitudinal profiles of the specimen with increasing u/H are presented in Fig. 6b. As for the empty honeycomb, longitudinal stretching of walls of the filled honeycomb is evident from the outlines in Fig. 6b. In fact, the longitudinal profiles of the empty and filled honeycombs are qualitatively very similar; compare Figs. 4b and 6b. However, the measured $F/(WH)$ versus u/H responses of the empty and filled honeycomb is markedly different with the filled honeycomb as seen from Fig. 5a where we have included the representative measurement of the empty response from Fig. 3a. Not only is the filled specimen significantly stronger but also the filled specimens have a higher hardening rate. We hypothesize that these differences are associated with a change in the mode of crushing of the honeycomb with filling preventing the formation of crush bands; the simulations in Section 4 will be used to explore the details of the deformation mechanisms.

We note in passing that the epoxy end caps of the filled tubes provide additional constraint to the deformation of the hexagonal honeycomb. To what extent does the presence of the end caps account for the elevation in tube strength rather than the presence of the gel-core? To assess this, additional tests were performed on an epoxy end-capped tube made from empty honeycomb and pinched using indenters of width $W/L = 0.25$. The compressive strength of this specimen is included in Fig. 5a and shows that the presence of the epoxy end-cap leads to a small constraint on the deformation mode of the empty honeycomb, but the effect is much less than the effect of gel-filling of the honeycomb.

A comparison between the measured pinching responses of the $W/L = 0.1$ filled and empty specimens is presented in Fig. 7a. The qualitative picture remains the same as the $W/L = 0.25$ case with the filled honeycomb displaying an approximately linear response and a hardening rate that is larger than that of the empty honeycomb. However, the differences between the filled and empty honeycomb responses are now smaller than that observed for the $W/L = 0.25$ case. This is because longitudinal stretching of the honeycomb walls now has a

larger contribution to the overall response and this stretching is approximately the same for both the empty and filled specimens.

4. Simulations and comparisons with observations

Three-dimensional (3D) Lagrangian finite element (FE) calculations were performed to simulate the experiments. The validated FE model is then exploited to develop an understanding of the deformation mechanisms of the filled honeycomb tubes.

4.1 Material models

The solid Al was modelled as an isotropic J2 flow theory solid with a Young's modulus $E_s = 69$ GPa, Poisson's ratio $\nu_s = 0.30$ and yield strength $\sigma_{Ys} = 210$ MPa. Mild strain hardening was included with the plastic strain ε_p versus stress σ relation given by

$$\varepsilon_p = 0.002 \left[\left(\frac{\sigma}{\sigma_{Ys}} \right)^n - 1 \right], \quad (1)$$

with the choice of the power law exponent $n = 7.5$ such that the strength increased to 290 MPa at a plastic strain of 0.018. The density of aluminium is assumed to be 2.7 Mg m^{-3} . These properties are representative of Al5052-H32 (Hatch (1984)).

The gel was chosen as a representative, almost incompressible solid of negligible shear strength compared to the uniaxial compressive strength of the empty hexagonal honeycomb. Preliminary compression tests on the gel revealed that it had a nominal compressive strength of 2 kPa at a nominal compressive strain of 0.5, with a J-shaped stress strain curve. Thus, the gel core has very low shear strength and closely resembles a fluid in its mechanical behaviour. For our purposes of modelling it within the Lagrangian setting, it suffices to treat the gel as an isotropic elastic, ideally plastic J2 flow theory solid but with a sufficiently low modulus and strength such that it behaves essentially as a fluid. Specifically, we assign the gel a modulus $E_c = 6.9$ MPa, Poisson's ratio $\nu_c = 0.4999$ and strength $\sigma_{Yc} = 0.025$ MPa. Additional calculations with $\sigma_{Yc} = 0.0025$ MPa were also performed, and these gave an almost identical load versus displacement curve of pinch response of gel-filled honeycomb. The density of the gel is assumed to be 1 Mg m^{-3} .

The epoxy end-plugs are modelled as an elastic solid, of Young's modulus 5 GPa and Poisson ratio 0.3. (This value of Young's modulus is typical of that for a structural epoxy.)

4.2 Finite element (FE) model

We report calculations on specimens with three types of honeycomb microstructure:

- (i) an *observed microstructure* created from a computer tomography micrograph of a honeycomb scanned prior to testing, see Fig. 1c;
- (ii) *perfect honeycombs* with all cell walls of length ℓ and inclinations $\omega = 30^\circ$ and 40° , see Fig. 1b; and
- (iii) *irregular honeycombs* constructed by randomly moving the nodes of the perfect microstructures of case (ii) by a distance 0.2ℓ in the $y - z$ plane.

In all cases the two cell walls of each hexagonal cell that are broadly in the y –direction had a thickness $2t$ and the remaining four walls had a thickness t with $t = 35 \mu\text{m}$. The cell wall length of the perfect honeycombs was selected as $\ell = 2 \text{ mm}$ which equals the average cell wall length in the observed microstructure. The resulting relative density is $\bar{\rho} = 0.027$ for $\omega = 30^\circ$ and $\bar{\rho} = 0.028$ for $\omega = 40^\circ$. The tubular specimens comprising 7×8 cells were constructed by ‘extruding’ the cross-sections to a length $L = 200 \text{ mm}$.

The FE calculations were performed using the explicit version of the general-purpose finite element package ABAQUS. The loading rate was sufficiently slow to ensure that inertial effects play a negligible role in all calculations reported here. The honeycomb was modelled in the FE model using 4-noded shell elements with reduced integration (S4R in the ABAQUS notation) with approximately 6 elements along the cell walls in the $y - z$ plane and an element of length 1 mm along the x –direction. Symmetry along the x – direction was exploited so that only half the span of the specimen was modelled. The loading indenters were modelled as analytical rigid surfaces with loading prescribed by imposing a relative displacement rate \dot{u} between the indenters. The frictionless general contact option in ABAQUS was used to model not only contact between the indenters and the specimen surfaces but also any possible contact that might occur between the honeycomb cell walls.

For modelling the filled honeycomb, the empty space within the cells of the honeycomb was filled with reduced integration hexahedral continuum elements (C3D8R in the ABAQUS notation) of size $0.4 \times 0.4 \times 1 \text{ mm}^3$. These 3D continuum elements were assigned the properties of the gel and of the epoxy adhesive to simulate the geometry in Fig. 2. Frictionless general contact was employed between the honeycomb and gel elements as well as the gel and epoxy adhesive while the elements modelling the adhesive were rigidly connected to the honeycomb. It is emphasised that the presence of the gel core constrains the overall volume of each tubular hexagonal cell of the specimen from dropping below its initial value upon pinching of the honeycomb-tube. However, the cross-sectional area of the honeycomb cells can dilate or shrink along the length of the honeycomb.

4.3 Comparison between measurements and simulations

The FE predictions are compared with the measured responses of the empty honeycombs in Figs. 3-4, and with the filled honeycombs in Figs. 5-7. The FE predictions for the observed microstructure of Fig. 1(b) is shown by dotted lines in the plots of Figs. 3, 5 and 7; predictions for the deformed shape of the honeycomb are given in Fig. 4 and 6 for the observed microstructure of Fig. 1(b).

First, consider the pinching response of the empty honeycomb. The FE predictions of the collapse response are in broad agreement with the measured values, including the scatter as a result of the geometric variability of honeycomb cross-section; the scatter in the FE results in Fig. 3b is predicted using the irregular honeycombs described in Section 4.2. A significant 3D reinforcement effect is present such that the pinch force is carried in part by axial membrane stresses within the cell walls external to the compressed section of the tube. The slope of the load versus displacement curve increases with increasing length of tube L in relation to the indenter width W , due to this membrane effect. Good agreement also exists between the predicted and observed deformation profiles of the empty honeycomb, as shown in Fig. 4.

Second, consider the collapse response of the gel-filled honeycombs. The load versus displacement behaviours are given in Fig. 5 for $W/L = 0.25$, and in Fig. 7 for $W/L = 0.1$. In both cases, the FE predictions of the collapse response are in broad agreement with the measured values, including the scatter modelled via the irregular honeycombs. A much stiffer response is evident for the gel-filled honeycomb than for the case of the empty honeycomb. Note the presence of load oscillations for the empty honeycomb, and a more stable response with no load oscillations for the filled honeycomb. There is also good agreement between the predicted and observed deformation profiles of the gel-filled honeycomb, see for example Fig. 6 for the choice $W/L = 0.25$.

Insight into the deformation mode of the empty and filled honeycomb is obtained by plotting in Fig. 8 the deformed cross-section of the honeycomb at mid-length of the tube, termed cross-section S_1 , and at a cross-section S_2 , positioned at quarter-length of the tube. The cross-sections are taken from the FE analysis, at selected values of $u/H = 0.05, 0.1$ and 0.15 , with $W/L = 0.25$.

There are striking differences in response for the empty and filled honeycombs. Most markedly, the empty honeycomb at cross-section S_1 beneath the indenter forms a series of crush bands and the formation of each is associated with an oscillation in load. The empty honeycomb remains predominantly elastic at cross-section S_2 up to $u/H = 0.15$. In contrast, the gel-filled honeycomb compresses in a relatively uniform manner with no crush band formation at section

S_1 , and at section S_2 the honeycomb inflates under the internal pressure of the gel core. To make this precise, the pressure distribution in the gel core at section S_1 is plotted in Fig. 9a for $u/H = 0.05, 0.1$ and 0.25 , again for the choice $W/L = 0.25$. Note that the low shear strength of the core implies that this pressure is almost constant over the length of each cell but can vary from cell to cell.

The cross-sectional area A of 3 representative honeycomb cells at sections S_1 and S_2 are plotted as a function of displacement u/H in Fig. 9b for the same FE simulation. For each cell, the area is normalised by its initial value A_0 . Upon taking Figs. 8 and 9 together, it is clear that the gel core is squeezed from the loaded portion (section S_1 , for example) to the outer portion at section S_2 such that the honeycomb at section S_1 deflates, while that at section S_2 it inflates. The cell walls in the outer portion rotate until the honeycomb adopts the shape close to that of a perfect hexagonal honeycomb, with inclined struts at an angle $\omega = 30^\circ$. The honeycomb with $\omega = 30^\circ$ is an extremal microstructure such that the cross-sectional area of a honeycomb of fixed cell wall lengths is maximised at $\omega = 30^\circ$ (Tankasala et al., 2021). Any further inflation of the honeycomb after the cell walls have rotated to $\omega = 30^\circ$ requires stretching of the cell walls. This implies that, after rotation of the cell walls of the outer honeycomb to $\omega = 30^\circ$, the outer honeycomb material switches into a much stronger stretching mode of its in-plane ($y - z$ plane) deformation, and a gel pressure (back-pressure) is generated. In turn, this increased back pressure elevates the compressive strength in the pinched zone. Post lock-up of the hexagonal cells at section S_2 , the hexagonal cells at section S_1 can no longer deform in an in-plane bending mode as large axial forces in the cell walls are needed to balance the gel pressure in the z -direction. Thus, the mode at section S_1 also switches into a strong in-plane stretching mode that is reminiscent of the mode B collapse response detailed by Tankasala et al. (2021).

In summary, the overall 3D collapse mode of the gel-filled honeycomb involves cooperative deformation of the cross-section S_1 involving cell deflation and deformation of the cross-section S_2 involving inflation, with cross-talk between the two regions of the tube due to axial flow of the gel. At a sufficiently large value of u/H , the plastic collapse mode at both sections S_1 and S_2 switches from a weak in-plane bending mode to a much stronger in-plane stretching mode.

5. Discussion

Our combined experimental and numerical study highlights the fact that the filling of a hexagonal honeycomb by an incompressible core of negligible deviatoric strength has a major effect upon the in-plane compressive strength of the honeycomb. The recent study by Tankasala

et al (2021) has highlighted the fact that incompressibility of the core can switch off the weak, bending modes of in-plane honeycomb response, and instead give rise to a much stronger stretching mode. The 3D geometry of the present study allows for cross-flow of the gel core from the zone directly beneath the loading platens to the outer zone, and so the fully constrained, incompressible 2D response is not achieved. However, a dramatic change in deformation mode is observed. It is thus instructive to investigate the effect of axial flow of the gel from the section S_1 to the section S_2 in the gel-filled hexagonal tube. We do this by comparing the predicted 3D pinching response of the hexagonal tube with the plane strain 2D response of the same gel-filled honeycomb.

Plane strain simulations (with deformation restricted to be in the $y - z$ plane) of the 2D uniaxial response have been performed on the observed honeycomb microstructure of Fig. 1c and the comparison with the pinching behaviour is shown in Fig. 10. Initially, at displacements u/H less than 0.15, the 3D pinching response is stronger than that of the 2D section, and this is attributed to the additional strength due to axial membrane stretching of the deformed tube. The pressure in the core of the 2D honeycomb remains small, as shown in Fig. 11, and this is attributed to a gap opening between the incompressible core and some of the faces of the honeycomb: recall that a contact algorithm is employed between the honeycomb and its core. The dilation of a hexagonal core upon compression can be understood upon noting that the cross-sectional area A of a hexagon of geometry in Fig. 1b is a maximum for $\omega = 30^\circ$, as mentioned above and explained in some detail by Tankasala et al (2021). The significance of this is seen as follows. Consider a hexagonal honeycomb with cell walls of initial inclination $\omega > 30^\circ$. Uniaxial compression of this honeycomb leads to an initial plastic collapse mode of the empty honeycomb: plastic hinges form at the vertices, ω decreases and the honeycomb dilates with the gel core playing no role as gaps open between the gel and the honeycomb cell walls. With continued rotation such that $\omega < 30^\circ$, the honeycomb shrinks again until it attains its initial value of cross-sectional area. Thereafter, volumetric lock-up ensues in the 2D case, and the honeycomb deforms by cell wall stretching in addition to bending. This lock-up phenomenon is evident in Figs. 10 and 11 for $u/H > 0.15$. In contrast, axial flow of the gel can continue to occur along the axis of the 3D tube, and so lock-up is not attained at section S_1 although the back-pressure due to the stretching of the cell walls at section S_2 does result in a hardening response. Consequently, for $u/H > 0.15$ the deformation of the 2D filled honeycomb is much more constrained and thus it becomes much stronger than the 3D pinched tube.

The sensitivity of pinching response of gel-filled tubes to inclination ω of the perfect hexagon has been explored by additional FE simulations, and the responses are plotted in Fig. 12. For the choice $\omega = 40^\circ$, as u/H increases from zero, the angle ω of the honeycomb at section S_2 decreases until volumetric lock-up occurs at approximately $\omega = 20^\circ$. Gel flow from the section S_1 to S_2 generates a much larger back pressure and the pinching stress sharply increases. Alternatively, consider the geometry for which $\omega = 30^\circ$, initially. Then, lock-up of the outer section S_2 occurs almost immediately and a much stiffer macroscopic pinching response occurs. If instead, the honeycomb has a random distribution of nodal positions about an initial, unperturbed value of $\omega = 40^\circ$ or $\omega = 30^\circ$, then cell-by-cell volumetric lock-up is progressive in nature and the pinching strength shows a less steep upturn within increasing u/H .

The findings of the present study allow us to interpret the previous compression tests by of D'Mello and Waas (2013) on a PDMS-filled PC honeycomb. They found that the compressive response of the PDMS adhesive alone much exceeds that of the empty honeycomb, and consequently the composite response is close to affine in nature, as dictated by the incompressible PDMS, with the PC tubes acting as a reinforcement fabric. This is transparent by comparing Figs. 4 and 12 of D'Mello and Waas (2013): the compressive stress versus strain response of the PDMS alone in their Fig. 12 is J-shaped (as expected for an elastomer); likewise, the compressive response of the filled honeycomb is J-shaped up to the point of vertical crack formation in the PC honeycomb, see their Fig. 4. The PC tubes are loaded in tension in the transverse direction due to the transverse extension imposed by overall incompressibility. D'Mello and Waas (2013) noted that vertical cracks form by the transverse failure of the filled honeycomb, and the emergence of these cracks dictated the compressive strength of the filled honeycomb. They also noted that the load response of the filled honeycomb much exceeded the sum of the two individual load responses of the unfilled honeycomb and of the PDMS alone. The reason for this synergistic effect is that the empty honeycomb collapses in a weak mode by cell wall bending whereas the filled honeycomb deforms by cell wall stretching.

6. Conclusions

The present study is a combined experimental and numerical analysis to determine the sensitivity of the compressive collapse response of a hexagonal honeycomb to the addition of a weak, incompressible core. A dramatic change in collapse mode occurs from unstable, crush band formation to a much more stable, hardening response. A new test geometry in the form of a gel-filled hexagonal tube has been designed, with pinch-like loading at mid-length. The tube has the

features of an energy absorbing device: when it is pinched at mid-length, the hexagonal honeycomb dissipates plastic work in the pinched zone and external to the pinched zone. The details of the collapse response, and in particular the lock-up displacement, are sensitive to the microstructure of the honeycomb, as illustrated in Fig. 12. Our study shows that the addition of an incompressible core has a major effect upon the in-plane compression response of a hexagonal honeycomb, and upon the pinching response of a hexagonal honeycomb in the form of an end-sealed tube.

Acknowledgements

The authors are grateful for financial support from the European Research Council in the form of an Advanced Grant (MULTILAT, 669764).

References

- Hatch, J.E. (1984). Aluminum, Properties and Physical Metallurgy. *American Society for Metals*.
- D’Mello, R. J. and Waas, A. M. (2013). Inplane crush response and energy absorption of circular cell honeycomb filled with elastomer. *Composites Structures*, **106**, 491-501.
- Gibson, L. J. and Ashby, M. F. (1997). Cellular solids, structure and properties. 2nd. Edn. Cambridge University Press.
- Kyriakides, S. (1993). Propagating instabilities in structures. *Advances in Applied Mechanics*, (ed. J W Hutchinson and T Y Wu), **30**, 67-189. Academic Press, Boston.
- Mozafari, H., Molatefi, H., Crupi, V., Epasto, G. and Guglielmino, E. (2015). In plane compressive response and crushing of foam filled aluminum honeycombs, *J. Compos. Mater.*, **49**(26), 3215-3228.
- Papka, S. D. and Kyriakides, S. (1994). In-plane compressive response and crushing of honeycomb. *J. Mech. Phys Solids*, **42**(10), 1499-1532.
- Papka, S. D., and Kyriakides, S. (1998). Experiments and full-scale numerical simulations of in-plane crushing of a honeycomb. *Acta Materialia*, **46**(8), 2765–2776.

Tankasala, H.C., Deshpande, V.S. and Fleck, N.A. (2021). The in-plane elastic-plastic response of an incompressible, filled honeycomb. *J. Mech. Phys. Solids*, **155**, 104536.

Triantafyllidis, N. and Schraat, M.W. (1998). Onset of failure in aluminum honeycombs under general in-plane loading, *J. Mech. Phys. Solids*, **46**(6), 1089-1124.

Vaziri, A., Xue, Z. and Hutchinson, J.W. (2006). Metal sandwich plates with polymer foam-filled cores, *J. Mech. Mater. Struct.*, **1**(1), 97–127.

Figure Captions

Fig. 1. Sketch of the pinching test setup. (a) isometric view; (b) end view; (c) representative CT-scan cross-section image.

Fig. 2. Sketch of the gel-filled end-plugged honeycomb specimens geometry prepared for pinching test. All dimensions are in mm.

Fig. 3. Load versus displacement response of pinched tube containing empty honeycomb, for $W/L=0.05, 0.1, 0.25$ and for uniaxial compression. Both measurements and finite element predictions are given. The solid lines give a representative measurement for each value of W/L . The dotted lines give the FE prediction for the observed microstructure of Fig. 1c. (a) Results, with scatter in experiments displayed; (b) results, with scatter in predictions displayed.

Fig. 4. (a) Side view of the pinched tube containing empty honeycomb at start of test; (b) deformed longitudinal profile of pinched tube for $W/L=0.25$. Both observed and predicted profiles are shown. The predictions assume the observed microstructure of Fig. 1c.

Fig. 5. Load versus displacement response of pinched tube containing a gel-filled honeycomb, for $W/L=0.25$. Both measurements and finite element predictions are given. The solid lines give a representative measurement. The dotted lines give the FE prediction for the observed microstructure of Fig. 1c. (a) Results, with scatter in experiments displayed; (b) results, with scatter in predictions displayed.

Fig. 6. (a) Side view of the pinched tube containing gel-filled honeycomb at start of test; (b) deformed longitudinal profile of pinched tube for $W/L=0.25$. Both observed and predicted profiles are shown. The predictions assume the observed microstructure of Fig. 1c.

Fig. 7. Load versus displacement response of pinched tube containing a filled honeycomb, for $W/L=0.1$. Both measurements and finite element predictions are given. The solid line gives a representative measurement. The dotted lines give the FE prediction for the observed microstructure of Fig. 1c. (a) Results, with scatter in experiments displayed; (b) results, with scatter in predictions displayed.

Fig. 8. Comparison between cross-sectional profiles for empty and filled honeycombs, for $W/L=0.25$, imaged at $u/H=0.05, 0.15$ and 0.25 . (a) at central cross-section S_1 ; (b) at S_2 halfway between the centre and end of the tube. The predictions assume the observed microstructure of Fig. 1c.

Fig. 9. (a) Finite element predictions of pressure at central cross-sections of filled honeycombs with $W/L=0.25$ at $u/H=0.05, 0.15$ and 0.25 ; (b) evolution of A/A_0 with increasing u/H of indicated cells in the filled honeycomb at central cross-section S_1 (solid line) and section S_2 , halfway between the centre and end of the tube (broken line). The predictions assume the observed microstructure of Fig. 1c.

Fig. 10. Finite element prediction of the effect of varying W/L upon the load versus displacement response of filled honeycombs. Predictions are included for the 2D in-plane response, in plane strain, termed ‘uniaxial’, for both the empty and gel-filled honeycomb. All predictions assume the observed microstructure of Fig. 1c.

Fig. 11. Finite element prediction of pressure of gel-filled 2D honeycomb subjected to uniaxial deformation, in plane strain. The predictions assume the observed microstructure of Fig. 1c.

Fig. 12. Finite element prediction of the effect of randomisation of initially perfect honeycomb with $\omega = 30^\circ$ (blue) and $\omega = 40^\circ$ (orange) upon the load versus displacement response of pinched tube containing a filled honeycomb, and $W/L=0.25$. Solid lines show the response of the perfect honeycomb and shaded areas show the envelope of randomly perturbed specimens in which all vertices are displaced 0.2ℓ .

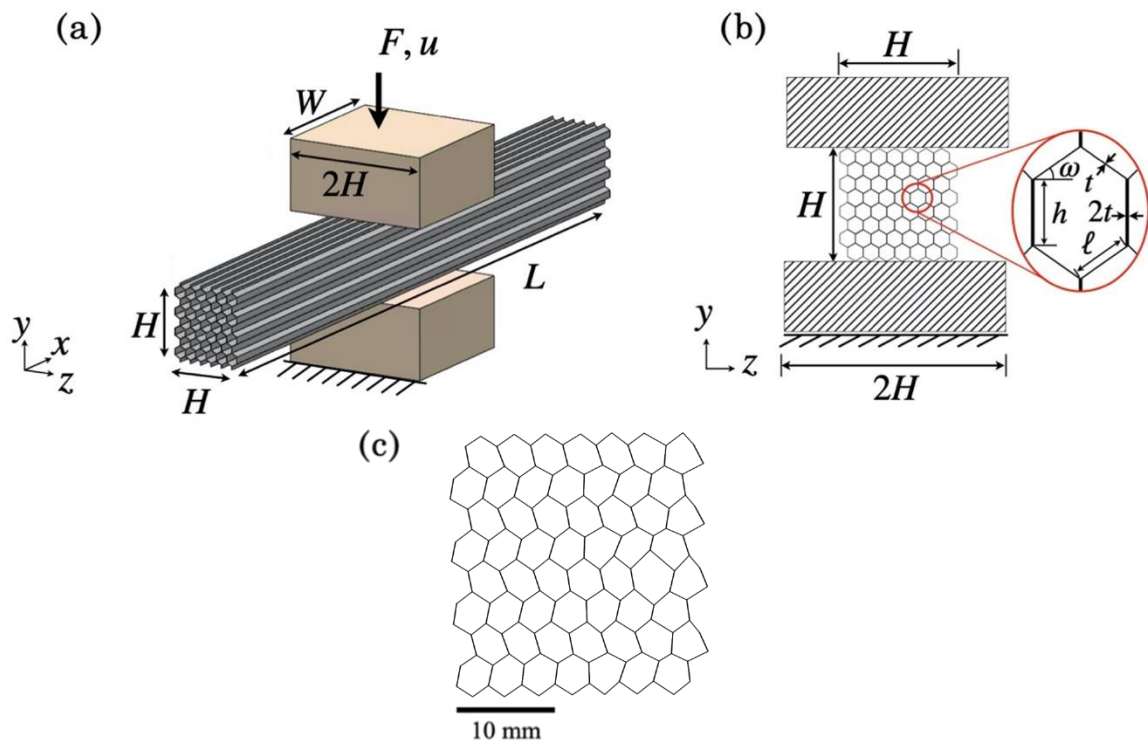


Fig. 1. Sketch of the pinching test setup. (a) isometric view; (b) end view; (c) representative CT-scan cross-section image.

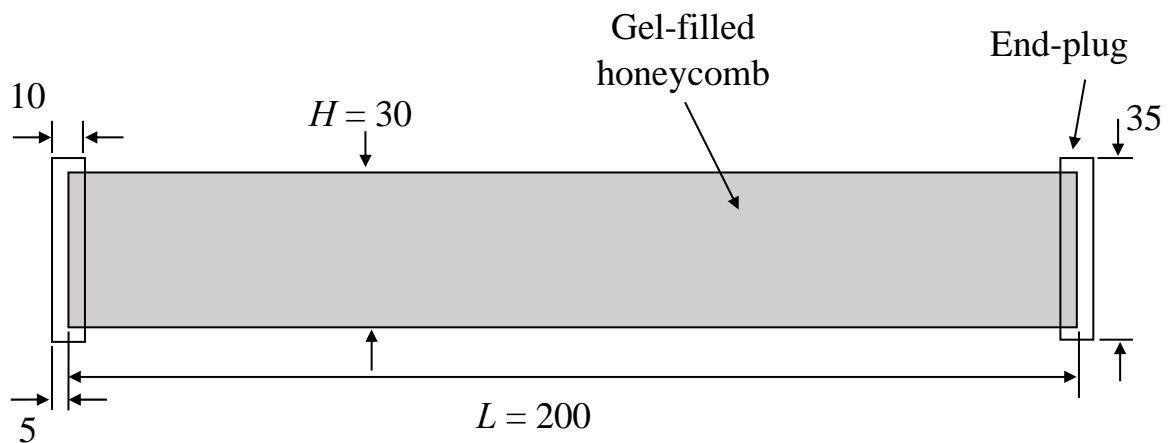


Fig. 2. Sketch of the gel-filled end-plugged honeycomb specimens geometry prepared for pinching test. All dimensions are in mm.

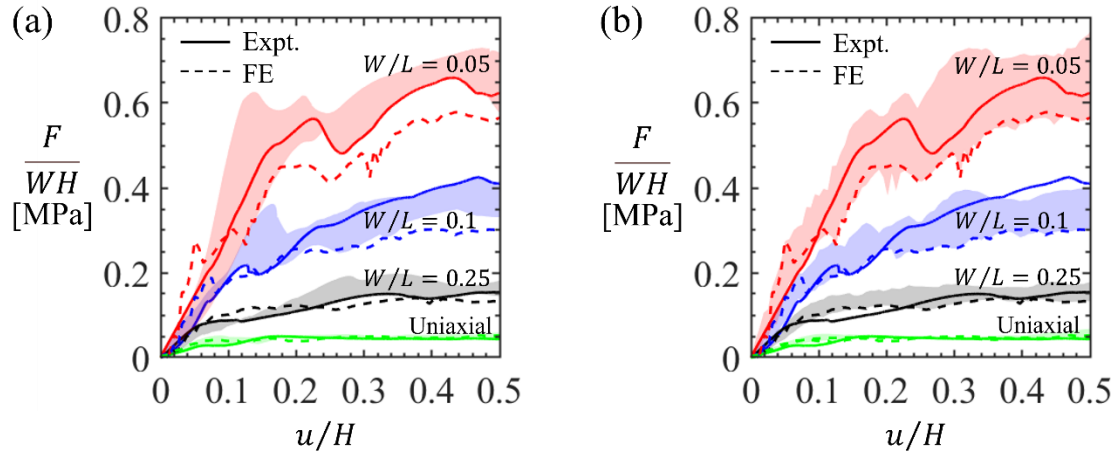


Fig. 3. Load versus displacement response of pinched tube containing empty honeycomb, for $W/L=0.05, 0.1, 0.25$ and for uniaxial compression. Both measurements and finite element predictions are given. The solid lines give a representative measurement for each value of W/L . The dotted lines give the FE prediction for the observed microstructure of Fig. 1c. (a) Results, with scatter in experiments displayed; (b) results, with scatter in predictions displayed.

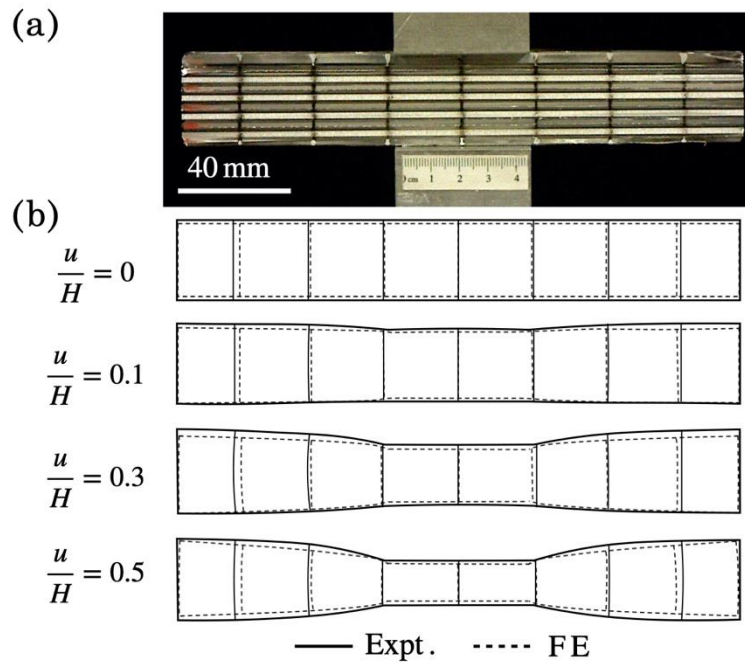


Fig. 4. (a) Side view of the pinched tube containing empty honeycomb at start of test; (b) deformed longitudinal profile of pinched tube for $W/L=0.25$. Both observed and predicted profiles are shown. The predictions assume the observed microstructure of Fig. 1c.

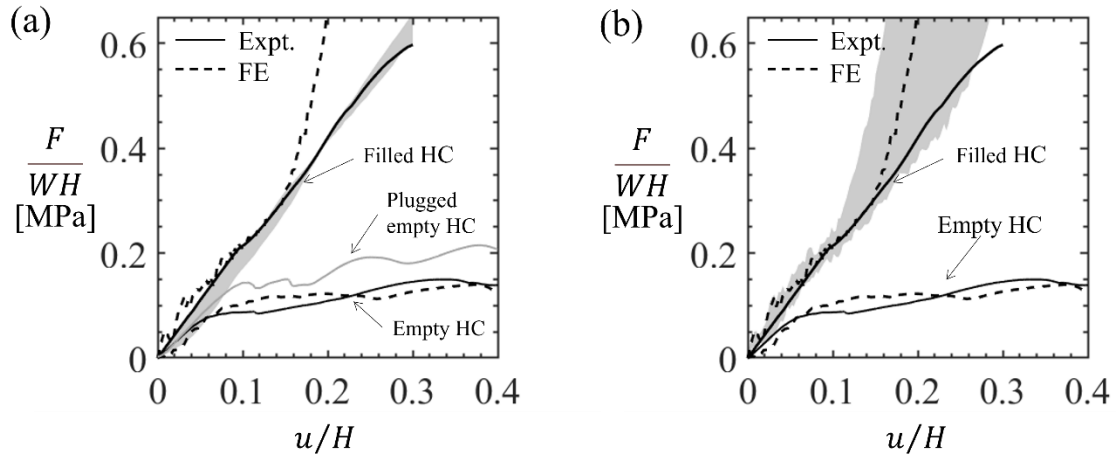


Fig. 5. Load versus displacement response of pinched tube containing a gel-filled honeycomb, for $W/L=0.25$. Both measurements and finite element predictions are given. The solid lines give a representative measurement. The dotted lines give the FE prediction for the observed microstructure of Fig. 1c. (a) Results, with scatter in experiments displayed; (b) results, with scatter in predictions displayed.

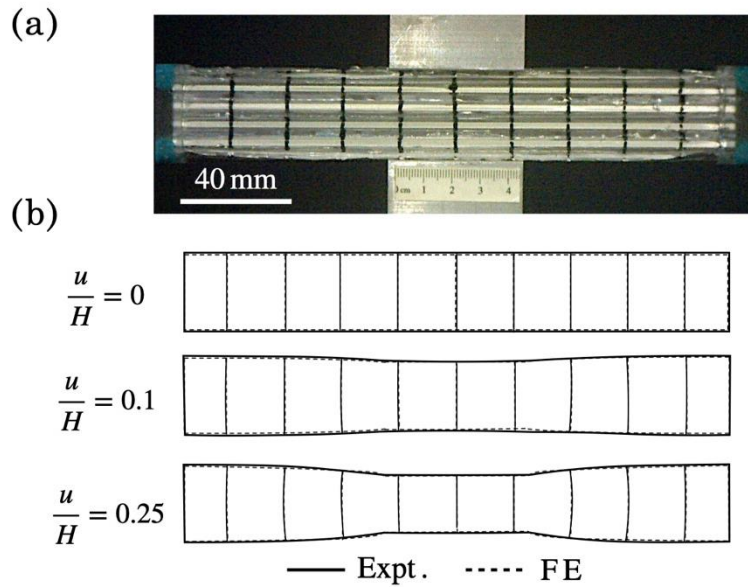


Fig. 6. (a) Side view of the pinched tube containing gel-filled honeycomb at start of test; (b) deformed longitudinal profile of pinched tube for $W/L=0.25$. Both observed and predicted profiles are shown. The predictions assume the observed microstructure of Fig. 1c.

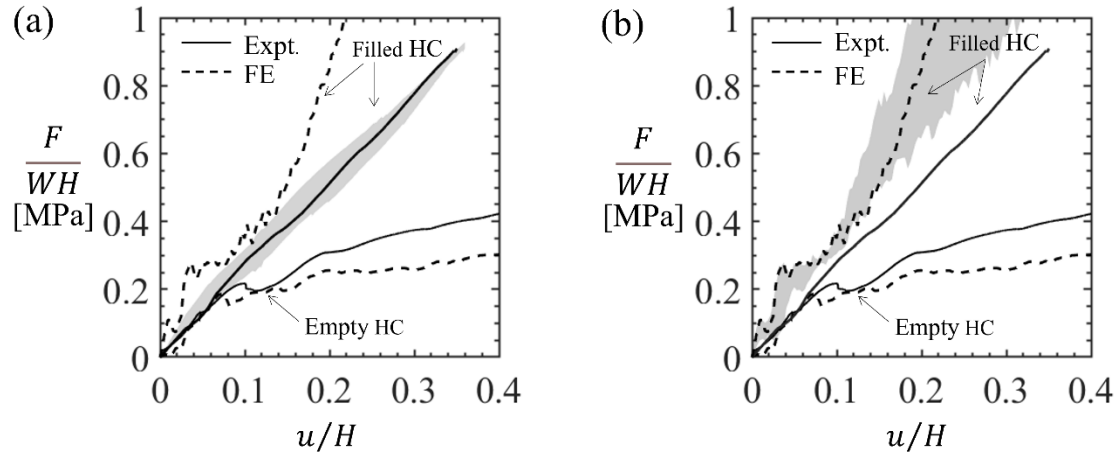
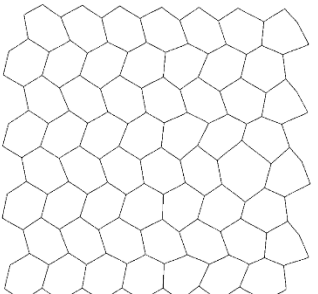
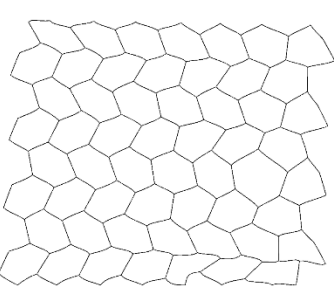
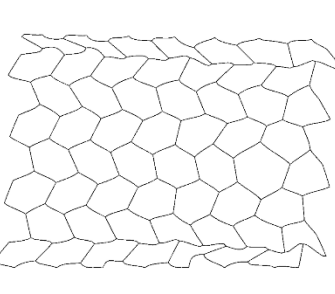
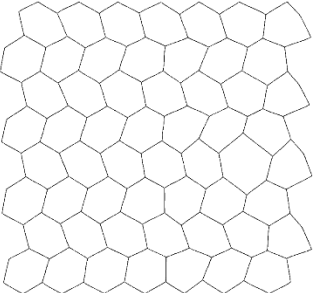
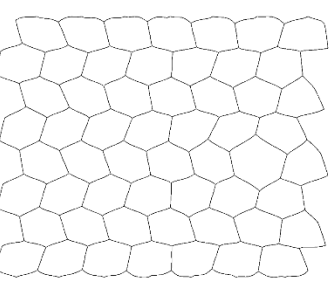
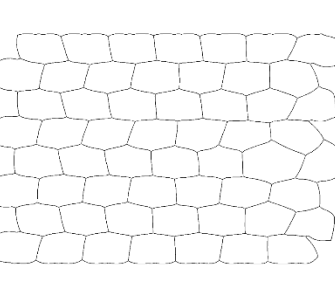


Fig. 7. Load versus displacement response of pinched tube containing a filled honeycomb, for $W/L=0.1$. Both measurements and finite element predictions are given. The solid line gives a representative measurement. The dotted lines give the FE prediction for the observed microstructure of Fig. 1c. (a) Results, with scatter in experiments displayed; (b) results, with scatter in predictions displayed.

(a)

| S_1 | $u/H=0.05$ | $u/H=0.15$ | $u/H=0.25$ |
|--------|---|--|---|
| Empty |  |  |  |
| Filled |  |  |  |

(b)

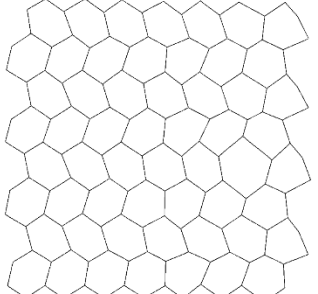
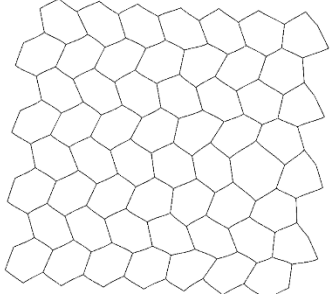
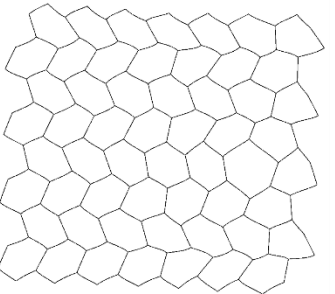
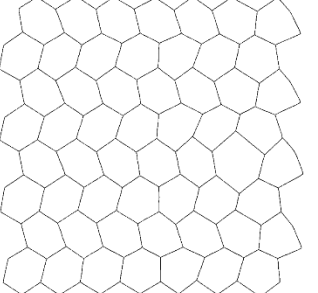
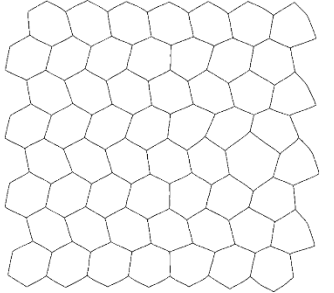
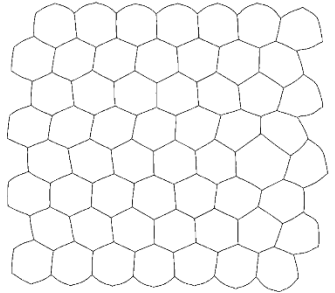
| S_2 | $u/H=0.05$ | $u/H=0.15$ | $u/H=0.25$ |
|--------|---|--|---|
| Empty |  |  |  |
| Filled |  |  |  |

Fig. 8. Comparison between cross-sectional profiles for empty and filled honeycombs, for $W/L=0.25$, imaged at $u/H=0.05, 0.15$ and 0.25 . (a) at central cross-section S_1 ; (b) at S_2 halfway between the centre and end of the tube. The predictions assume the observed microstructure of Fig. 1c.

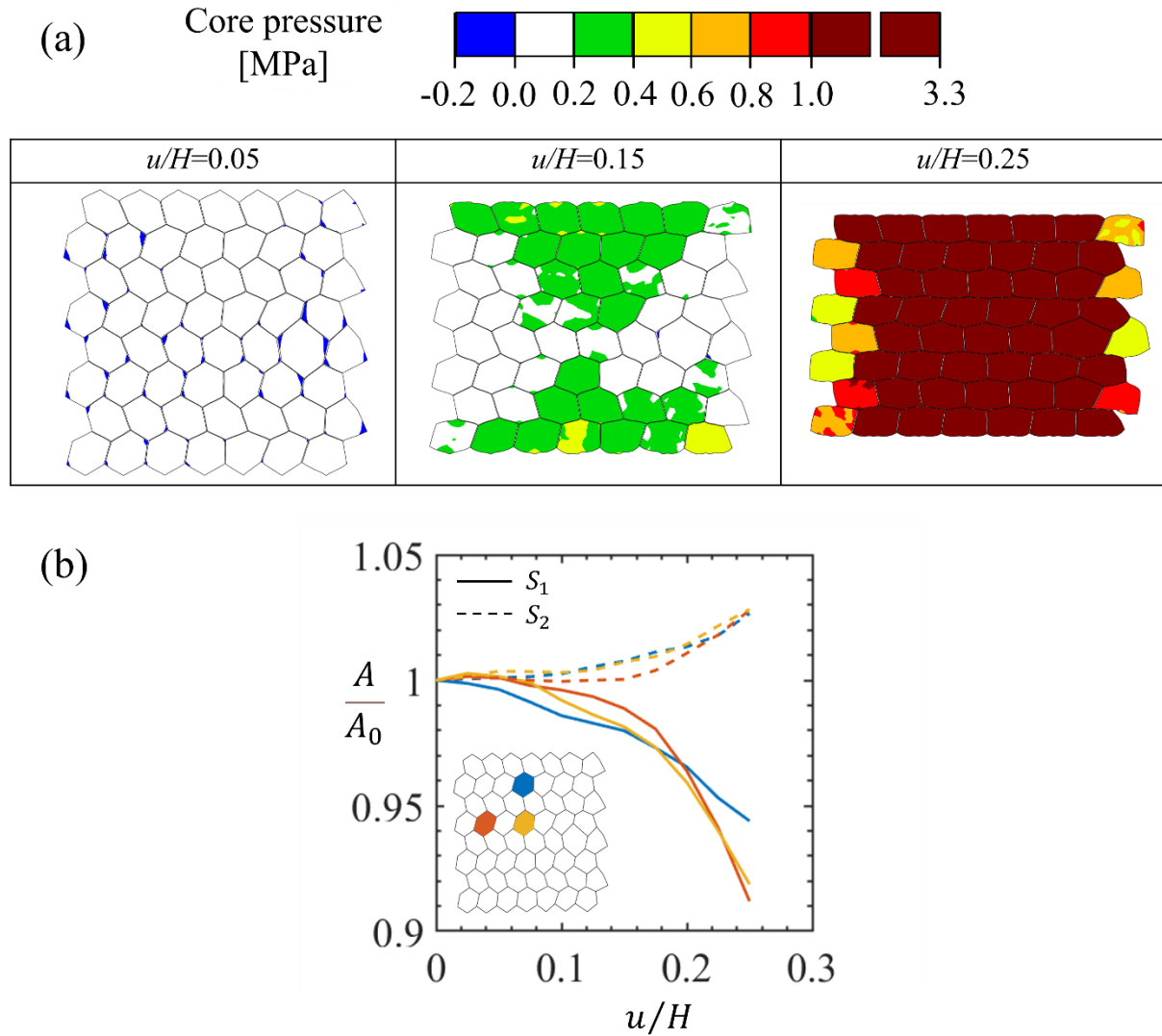


Fig. 9. (a) Finite element predictions of pressure at central cross-sections of filled honeycombs with $W/L=0.25$ at $u/H=0.05$, 0.15 and 0.25 ; (b) evolution of A/A_0 with increasing u/H of indicated cells in the filled honeycomb at central cross-section S_1 (solid line) and section S_2 , halfway between the centre and end of the tube (broken line). The predictions assume the observed microstructure of Fig. 1c.

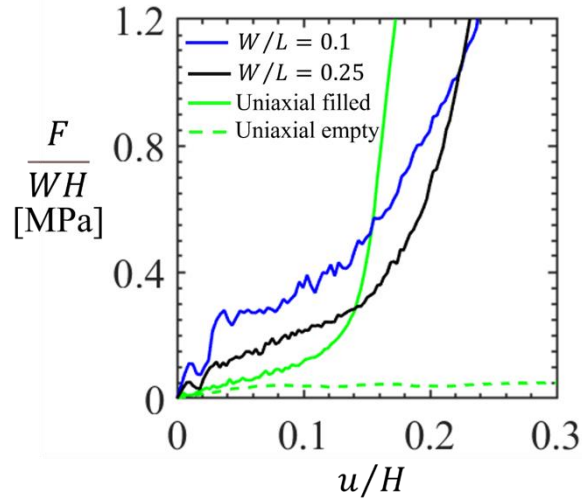


Fig. 10. Finite element prediction of the effect of varying W/L upon the load versus displacement response of filled honeycombs. Predictions are included for the 2D in-plane response, in plane strain, termed ‘uniaxial’, for both the empty and gel-filled honeycomb. All predictions assume the observed microstructure of Fig. 1c.

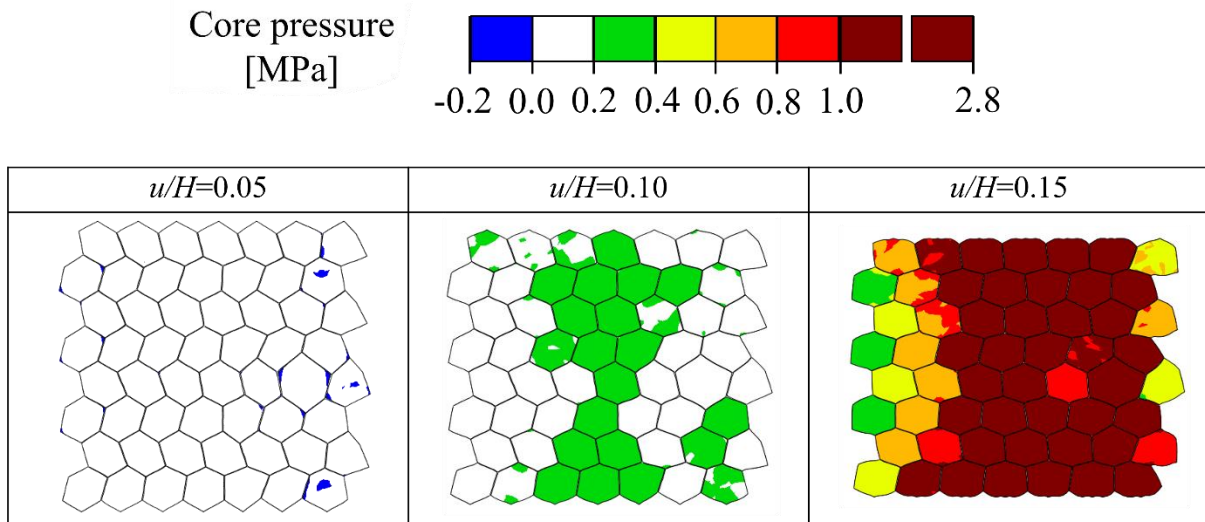


Fig. 11. Finite element prediction of pressure of gel-filled 2D honeycomb subjected to uniaxial deformation, in plane strain. The predictions assume the observed microstructure of Fig. 1c.

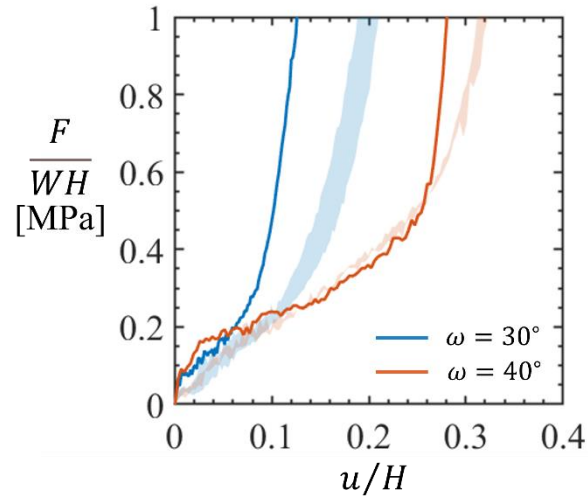


Fig. 12. Finite element prediction of the effect of randomisation of initially perfect honeycomb with $\omega = 30^\circ$ (blue) and $\omega = 40^\circ$ (orange) upon the load versus displacement response of pinched tube containing a filled honeycomb, and $W/L=0.25$. Solid lines show the response of the perfect honeycomb and shaded areas show the envelope of randomly perturbed specimens in which all vertices are displaced 0.2ℓ .